Hindawi
Scientific Programming
Volume 2021, Article ID 6256562, 10 pages
https://doi.org/10.1155/2021/6256562

Research Article

Relationship between Twin-to-Twin Selective Intrauterine Growth Restriction with sFas/sFasL Level of Umbilical Cord Blood Using Doppler Ultrasound Fetal Heart Rhythm Detection Algorithm

Gaibian Zhu, Qiuyan Zhang, and Sujuan He

Department of Obstetrics and Gynecology, Maternal and Child Health Hospital, Shanxi Children's Hospital, Taiyuan 030006, Shanxi, China

Correspondence should be addressed to Sujuan He; 2016101009@stu.gzucm.edu.cn

Received 19 September 2021; Revised 1 December 2021; Accepted 3 December 2021; Published 20 December 2021

Academic Editor: M Pallikonda Rajasekaran

The study focused on the application value of ultrasound Doppler fetal heart rate detection algorithm based on short-time Fourier transform (STFT) in the diagnosis of twin-to-twin selective intrauterine growth restriction (sIUGR) and the correlation between twin-to-twin sIUGR and sFas/sFasL levels of umbilical cord blood. The normalized method was introduced into the STFT algorithm to optimize it to detect the fetal instantaneous heart rate. 82 pregnant women with twin pregnancies were selected as the research subjects and they were divided into the restricted group (41 cases) and the control group (41 cases) according to whether the fetus had selective growth restriction. The two groups were compared for the differences in the fetal mortality, complication rate, and sFas/sFasL expression levels. The results showed that the STFT-based ultrasonic Doppler fetal heart rate detection algorithm could ensure the quality of the fetal heart rate signal and had high resolution at the 200–400 Hz characteristic frequency band and that the accuracy in distinguishing S1 and S2 was 5.8% higher than that of the traditional autocorrelation algorithm. The proportion of abnormal fetal heart rate in the restricted group was significantly higher than that in the control group ($P < 0.05$), birth weight was significantly lower than that in the control group ($P < 0.05$), and fetal mortality was significantly higher than that in the control group ($P < 0.05$). There was no statistical difference in the incidence of complications between the two groups ($P > 0.05$). In restricted group, the content of sFas in cord blood was (3326.54 ± 317.42) pg/mL and that in the control group was (2003.29 ± 196.45) pg/mL. The content of sFas in cord blood of the restricted group was significantly higher than that of the control group ($P < 0.01$). In the restricted group, the content of sFasL in cord blood was (382.52 ± 36.17) pg/mL, and that in the control group was (180.84 ± 16.20) pg/mL. The content of sFasL in cord blood of the restricted group was significantly higher than that of the control group ($P < 0.001$). It was concluded that the STFT-based ultrasound Doppler fetal heart rate monitoring is beneficial to early diagnosis and timely intervention of twin-to-twin sIUGR.

1. Introduction

With the continuous development of assisted reproductive technology, the incidence of twin-to-twin pregnancy has shown a significant upward trend, from 1/80 of natural pregnancy to about 20% [1]. The intrauterine growth environment of twin-to-twin pregnancy is more complicated than a single pregnancy, and the incidence of premature delivery, intrauterine growth restriction, perinatal mortality, and congenital turbulence is significantly increased [2]. Fetal growth restriction (FGR) is one of the important complications of the perinatal period, with an incidence rate of 2.75%~15.53%, and the domestic average FGR incidence rate is 6.39% [3]. FGR has a certain impact on fetal development and later physical and intellectual development, and its perinatal mortality rate is about 5 times that of normal fetuses [4], so it is of great significance to explore the pathogenesis of FGR. There are many and complex causes of

FGR. The Fas/FasL system is mainly responsible for inducing cell apoptosis. The current research results show that Fas and FasL are expressed in placental trophoblasts and decidua cells of full-term parturients. Fas and FasL expression changes after pregnancy, which has a certain protective effect on the fetus. Studies have analyzed the Fas/FasL expression in the placenta of FGR patients and normal pregnant women. The results found that the Fas expression of FGR patients was significantly higher than that of normal pregnant women, while FasL expression was significantly lower than that of normal pregnant women, indicating that Fas and FasL expression levels are associated with the occurrence of FGR [5]. However, there are few studies on the correlation between Fas/FasL and twin-to-twin selective intrauterine growth restriction (sIUGR).

Fetal heart rate monitoring is a common clinical method to ensure the safety of mothers and fetuses. The traditional fetal heart rate monitoring uses an autocorrelation algorithm to calculate the fetus's instantaneous heart rate, but it is susceptible to interference from maternal and fetal activities, sensors, and the external environment, so it is difficult to accurately measure the fetus's instantaneous heart rate [6]. Short-time Fourier transform (STFT) is a commonly used time-frequency analysis method, which is characterized by convenient analysis and is used for frequency positioning of sound signals [7]. Some researchers have applied STFT to the processing of fetal heart sound signals by ultrasonic Doppler. The results showed that this algorithm can overcome the weakness of fetal heart sound easily disturbed by noise, realize the real-time calculation of instantaneous heart rate of fetal heart sound, and improve the accuracy of fetal heart rate calculation. However, STFT cannot achieve high resolution in both frequency domain and time domain, so it needs to be further optimized.

Above, there are currently few studies on the correlation between Fas/FasL and twin-to-twin SIUGR, and the resolution of the STFT algorithm needs to be further improved. In this study, normalized image processing method was introduced based on STFT algorithm to improve the resolution of fetal heart rate by ultrasound Doppler. Meanwhile, 82 twin-to-twin pregnant women were taken as research subjects to explore the correlation between twin-to-twin sIUGR and the level of sFas/sFasL in cord blood, expected to provide a reference for the diagnosis and treatment of twin-to-twin sIUGR.

2. Materials and Methods

2.1. Research Subjects and the Grouping. 82 pregnant women who were diagnosed as having twin-to-twin selective fetuses in the obstetrics department of our hospital from February 2017 to December 2020 were selected as the research subjects, aged 25–39 years old, with an average age of (28.33 ± 4.53) years. According to whether the fetus has selective growth restriction, they were divided into the restricted group (41 cases) and control group (41 cases). Inclusion criteria for this study: (I) patients not accompanied by structural or chromosomal abnormalities; (II) all pregnancies were of natural fertilization. The exclusion criteria: (I) the presence of typical twin-to-twin transfusion syndrome; (II) those with fetal malformations during the prenatal examination. The study has been approved by the ethics committee of the hospital, and all subjects included in the study had signed an informed consent form.

2.2. Establishment of Optimized STFT Algorithm. The STFT establishes a bridge from the time domain to the frequency domain [8], and it is a commonly used time-frequency analysis method. It has the characteristics of strong matching ability, stable extraction of features, and high matching accuracy [9]. Assuming that the analyzed signal is $x(t)$, $t \in [-\infty, \infty]$, and the analysis window function is $w(t)$, then, for nonstationary signals $x(t)$, the STFT algorithm can be expressed as follows:

$$\mathrm{STFT}(t, w) = \int_{-\infty}^{\infty} [x(a) \cdot w(a - t)] e^{-a} \mathrm{d}a, \tag{1}$$

where $w(a - t)$ represents the analysis window $w(t)$ shifted from time 0 to time t. By windowing and truncating the original signal through $w(a - t)$, a short-term signal $x_i(a) = x(a) \cdot w(a - t)$ is obtained.

Assuming that the duration of the analysis window is Δt, the time of time-domain windowing and truncation is $[t - \Delta t/2, t + \Delta t/2]$. Then, the STFT at w can be expressed as follows:

$$\mathrm{STFT}(t, w) = e^{-wt} \frac{1}{2\pi} \int_{-\infty}^{\infty} [\hat{x}(a') w(w' - a)] e^{-at} \mathrm{d}a', \tag{2}$$

where $\hat{x}(a')$ is the spectrum of the analysis window; and $w(w' - a)$ represents the spectrum of the analysis window shifted from $a = 0$ to a $w(t)$; by windowing and truncating the signal spectrum through $w(w' - a)$, the short-frequency signal is calculated as follows:

$$\hat{x}_i(a') = \hat{x}(a') \hat{w}(w' - a). \tag{3}$$

Fourier transform is performed on the continuous signal $x(t)$ and windowing $v(t)$ is performed on the result $\mathrm{STFT}(t, w)$ of the continuous Fourier transform. Then, the inverse Fourier transform algorithm is expressed as follows:

$$v(t) = \frac{1}{2} \int \int \mathrm{STFT}[(t', a) v(t - t') \mathrm{d}t'] e^{at} \mathrm{d}a. \tag{4}$$

According to the $\mathrm{STFT}(t, w)$ algorithm, STFT can be expressed as follows:

$$y(t) = x(t) \int w(t) \mathrm{d}t. \tag{5}$$

To completely reconstruct the signal, the STFT should meet the following conditions:

$$\int w(t) v(t) \mathrm{d}t = 1. \tag{6}$$

When $v(t) = w(t)$, the STFT complete reconstruction condition can be expressed as follows:

$$\int |w(t)|^2 \mathrm{d}t = 1. \tag{7}$$

To realize discrete STFT, it is necessary to sample the STFT in the digital frequency domain and the corresponding STFT can be expressed as follows:

$$S_x(n,a) = \sum_{m=-\infty}^{\infty} x(m)w(n-m)e^{-am}, \tag{8}$$

where $w(n)$ represents the analysis window.

The frequency variable is continuous and the frequency variable needs to be discretized [10]. Then, the discrete STFT of the digital signal can be expressed as follows:

$$S_x(n,k) = \sum_{m=0}^{N-1} x(m)w(n-m)e^{-(2\pi 2mk/N)} \quad k = 0,\ 1,\ \ldots,\ N-1. \tag{9}$$

Then, the discrete STFT can be expressed as follows:

$$S_x(n,a) = \sum_{m=-\infty}^{\infty} x(n-m)w(m)e^{a(n-m)}. \tag{10}$$

For nonstationary signals $x(n)$, $n \in [-\infty, \infty]$, the window sequence is $w(n)$. Then, the sequence STFT algorithm transformation can be expressed as follows:

$$\mathrm{STFT}(n,\Omega) = \sum_{m} x(m)w(n-m)e^{-\Omega m}, \tag{11}$$

where $x(m)w(n-m)$ represents a short-time sequence, and the inverse transformation of $\mathrm{STFT}(n,\Omega)$ at time n can be expressed as follows:

$$\begin{aligned} x_n(m) &= x(m)w(n-m) \\ &= \frac{1}{2\pi}\int_{-\pi}^{\pi} \mathrm{STFT}(n,\Omega)e^{-\Omega m}\mathrm{d}\Omega. \end{aligned} \tag{12}$$

Suppose $w(0) \neq 0$, let $m = n$, and then the sequence STFT inverse transformation can be expressed as follows:

$$x(n) = \frac{1}{2\pi w(0)}\int_{-\pi}^{\pi} \mathrm{STFT}(n,\Omega)e^{-\Omega n}\mathrm{d}\Omega. \tag{13}$$

During the processing of the ultrasonic Doppler signal, the spectral shape and performance of the window function have a significant impact on the spectrum leakage and fence effect [11]. The rectangular window belongs to the zeroth power window of the time variable [12] and the discretized rectangular window of length N can be expressed as follows:

$$w_R(n) = \begin{cases} 1, & n = 0, 1, \ldots, N-1, \\ 0, & \text{other.} \end{cases} \tag{14}$$

Then, its discretization form can be expressed as follows:

$$W_R(w) = e^{-w((N-1)/2)}\frac{\sin(wN/2)}{\sin(w/2)}. \tag{15}$$

The triangular window is the first-order form of the power window [13] and the discretized rectangular window of length N (even number) is as follows:

$$w_{Tn}(n) = \begin{cases} \dfrac{2n}{N-2}, & n = 0, 1, \ldots, \dfrac{N}{2} - 1, \\ \dfrac{2n-4-2n}{N-2}, & n = \dfrac{N}{2}, \ldots, N-1. \end{cases} \tag{16}$$

Then, its discretization form can be expressed as follows:

$$w_{Tn}(w) = \frac{2e^{-Nw/2}}{N}\left[\frac{\sin(Nw/4)}{\sin(w/2)}\right]^2. \tag{17}$$

The time domain of the discrete Hanning window of length N is expressed as follows:

$$w_{Hn}(n) = \frac{1}{2} - \frac{1}{2}\cos\left(\frac{2\pi}{N}n\right) \quad n = 0, 1, \ldots, N-1. \tag{18}$$

The time-domain discretization form of the Hanning window can be expressed as follows:

$$_{Hn}(n) = \frac{1}{2}W_R(w) - \frac{1}{4}\left[W_R\left(w - \frac{2\pi}{N}\right) + W_R\left(w + \frac{2\pi}{N}\right)\right]. \tag{19}$$

The time-domain expression of the discrete Hamming window of length N is as follows:

$$w_{Hm}(n) = 0.54 - 0.46\cos\left(\frac{2\pi}{N}n\right) \quad n = 0, 1, \ldots, N-1. \tag{20}$$

The time-domain discretization form of Hamming window can be expressed as follows:

$$W_{Hm}(w) = 0.54W_R(w) - 0.23\left[W_R\left(w - \frac{2\pi}{N}\right) + W_R\left(w + \frac{2\pi}{N}\right)\right], \tag{21}$$

where $W_R(w)$ is the spectral function of the rectangular window.

Normalized cross-correlation (NCC) is one of the robust matching methods. It has the characteristics of strong antibackground noise, strong adaptability to image distortion, and high matching accuracy [14]. In the study, the normalization algorithm is introduced into STFT to optimize it. The normalized correlation coefficient between the

feature template M and the two-dimensional time-frequency diagram S in the two-dimensional time-frequency plane can be expressed as follows:

$$R(x, y) = \frac{\sum_{\mu=0}^{U=1}\sum_{v=0}^{V=1}[M(\mu, v) - c(M)]\left[S(x+\mu, y+v) - c\left(S_{xy}\right)\right]}{\sum_{\mu=0}^{U=1}\sum_{v=0}^{V=1}[M(\mu, v) - c(M)]^2\left[S(x+\mu, y+v) - c\left(S_{xy}\right)\right]^2}, \tag{22}$$

where $c(M)$ is the mean value of the template image, $c(S_{xy})$ means the mean value of the area of $U \times V$ with (x, y) as the starting point, and the template size is $U \times V$.

The one-dimensional vectors of the template M and the matched image area can be expressed as follows:

$$\begin{aligned} \mathrm{HM}(i) &= \{hm(i, j) - c(M), j = 0, 1, \ldots, V-1\}, \\ \mathrm{HS}_{xy} &= \left\{\mathrm{HS}_{xy}(i), i = 0, 1, \ldots, U-1\right\}, \end{aligned} \tag{23}$$

where HM is the template one-dimensional vector and HS_{xy} is the one-dimensional vector of the image area to be matched. Then, the template row vector can be expressed as $\mathrm{HM}(i) = \{hm(i, j) - c(M), j = 0, 1, \ldots, V-1\}$, the image area vector to be matched can be expressed as $\mathrm{HS}_{xy}(i) = \left\{hs_{xy}(i) - c(S_{xy}), j = 0, 1, \ldots, V-1\right\}$, and the normalized cross-correlation coefficient can be further expressed as follows:

$$R(x, y) = \frac{\sum_{i=0}^{U-1}\mathrm{Re}[\mathrm{HM}(i)], \mathrm{HS}_{xy}(i)}{\|\mathrm{HM}\|_2 * \left\|\mathrm{HS}_{xy}\right\|_2}, \tag{24}$$

where $\mathrm{Re}[\mathrm{HM}(i)], \mathrm{HS}_{xy}(i)$ represents the inner product of $\mathrm{HM}(i)$ and $\mathrm{HS}_{xy}(i)$; and $\|\mathrm{HM}\|_2$ and $\|\mathrm{HS}_{xy}\|_2$ represent the 2 norms of the sum.

In this study, the STFT algorithm is optimized by introducing the normalized algorithm. The flowchart of the fetal heart rate detection algorithm is shown in Figure 1.

2.3. Algorithm Operating Environment and sIUGR Evaluation Criteria. The optimized STFT algorithm to detect fetal instantaneous heart rate is programmed in MATLAB 7.11.0 and the operating environment is Windows XP. The sampling frequency of heart sounds is qq025 Hz, 14-bit A/D conversion is adopted, and the sampling data is transmitted to the upper computer through serial communication.

SIUGR diagnostic criteria [15]: the estimated weight of a fetus of twins is lower than the 10% of the fetus at normal gestational weeks and the twin-to-twin weight difference is more than 25%.

2.4. sFas/sFasL Level in Umbilical Cord Blood. In the second trimester of pregnancy, the two groups of pregnant women, 2 mL of umbilical cord blood was drawn under the guidance of B ultrasound, anticoagulated using heparin, and centrifuged to obtain plasma, which was stored at −20°C. The sFas/sFasL levels in the cord blood of the two groups of pregnant women were detected according to the instructions of the ELISA test kit (R&D System, USA).

2.5. Statistical Methods. The experimental data were processed using SPSS 19.0 statistical software, and the count data were tested by χ^2, and $P < 0.05$ indicates that the difference was statistically significant.

3. Results

3.1. The Optimized STFT Algorithm. Figure 2 shows the initial fetal heart sound data collected by Doppler ultrasound. This one-dimensional data cannot effectively display all the features of fetal heart sounds while the two-dimensional signal can, and it has a high resolution at 200~400 Hz, so in the follow-up research, the frequency band of 200~400 Hz was used.

After the original fetal heart rate signal map was normalized, the normalized correlation curve of the feature template and the target image is shown in Figure 3. It was noted that the relationship numbers were all above 0.86 at different times.

3.2. Fetal Heart Rate Detected by the Optimized STFT Algorithm. The fetal heart sound signals collected by Doppler ultrasound (Figure 4) were extracted by the autocorrelation algorithm and the optimized STFT algorithm, respectively. For the fetal heart signal with a small amplitude, autocorrelation cannot accurately locate it (Figure 5), only showing an abnormal fetal heart rate. The instantaneous heart rate extracted by the optimized STFT algorithm can accurately locate the fetal heart sound signal with a small amplitude and can correctly display the instantaneous fetal heart rate waveform (Figure 6).

The segmentation result of the fetal heart sound signal by the optimized STFT algorithm is shown in Figure 7. It was noted that the STFT optimization algorithm can accurately segment the S1 and S2 sounds of the fetal heart sound.

3.3. Fetal Heart Sound Detection Results by the Optimized STFT Algorithm. Figure 8 shows the detection results of clinically collected fetal heart sounds. For fetuses at 30–40 weeks of gestation, the autocorrelation algorithm [16] and optimized STFT algorithm were used to detect fetal heart sounds. The results showed that the detection error rate of the autocorrelation algorithm at 32 weeks and 38 weeks was 4% and 2%, respectively; those of the optimized STFT were 1% and 0, respectively, and the total detection error rate was reduced by 5%.

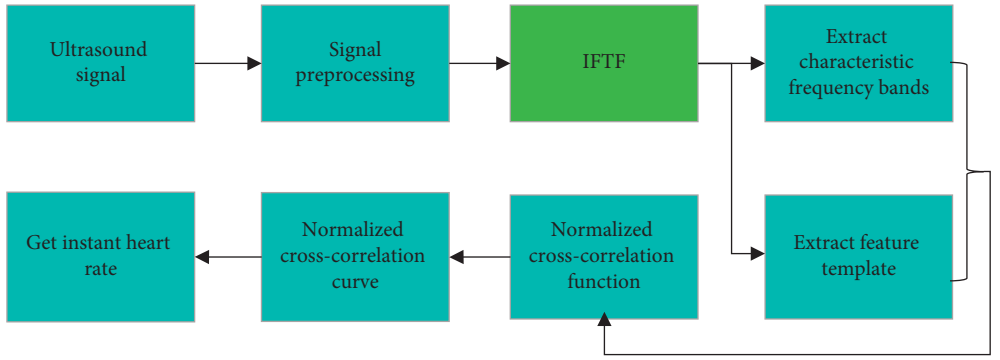

Figure 1: The flowchart of the optimized STFT algorithm to detect instantaneous heart rate.

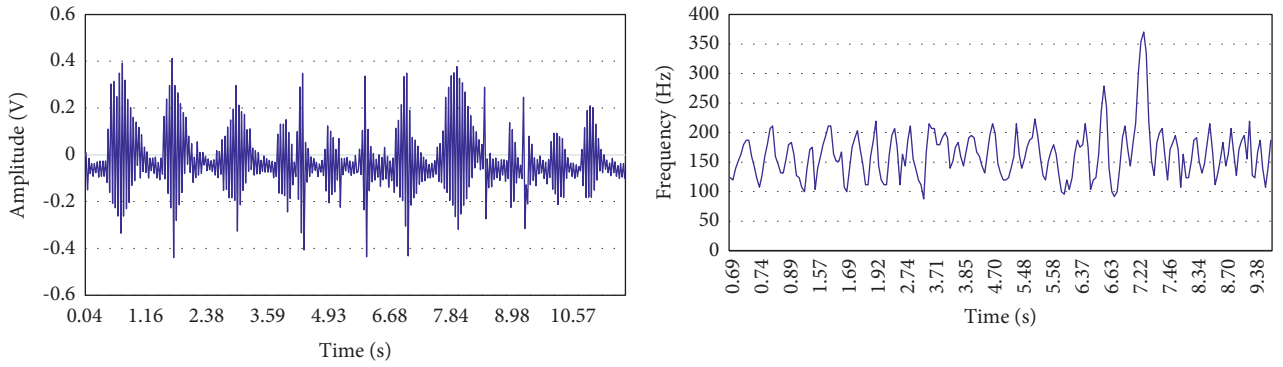

Figure 2: Ultrasound Doppler fetal heart sound signals. (a) Ultrasound Doppler fetal heart rate signals; (b) two-dimensional time-frequency contour graph of fetal heart rate.

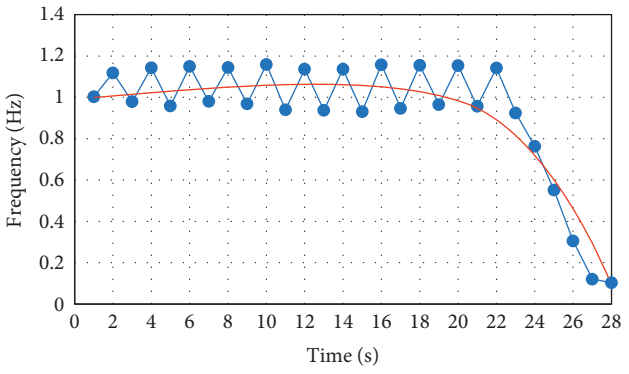

Figure 3: Normalized cross-correlation curve.

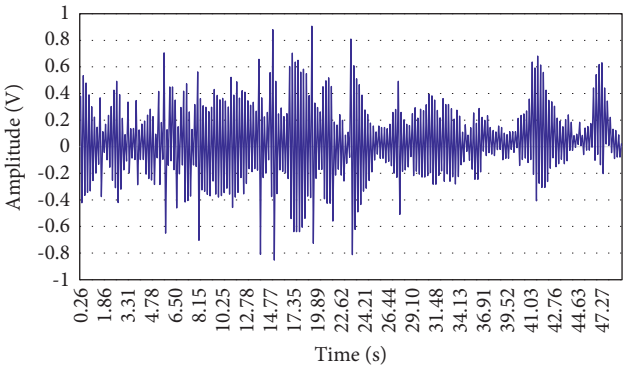

Figure 4: Fetal heart sound signals.

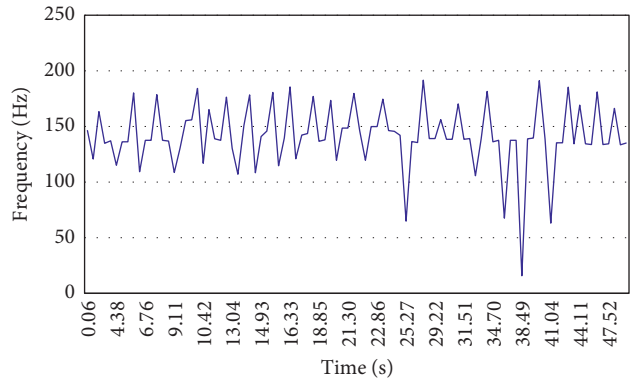

Figure 5: The instantaneous heart rate of fetal heart sounds extracted by the autocorrelation algorithm.

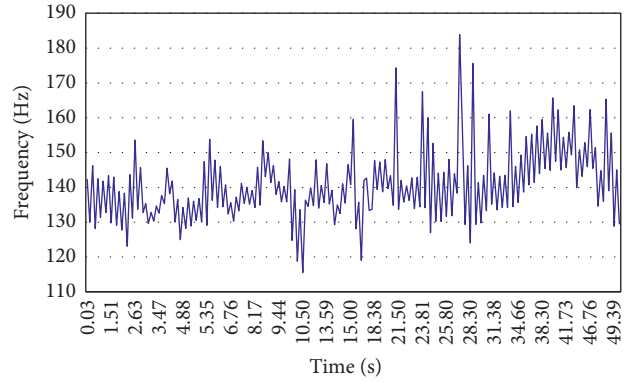

Figure 6: The instantaneous heart rate extracted by the STFT optimization algorithm.

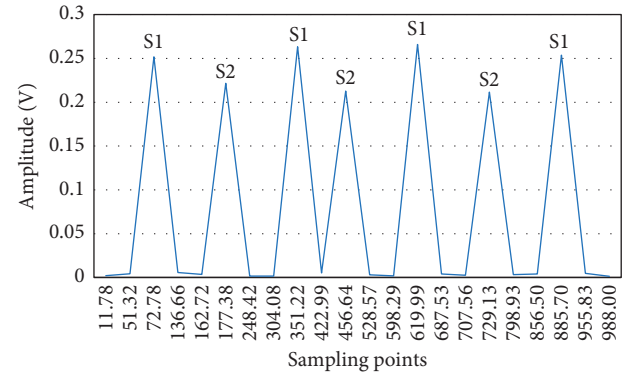

Figure 7: Segmentation results of features of fetal heart sounds.

3.4. Comparison of Basic Clinical Data of Two Groups of Pregnant Women. The restricted group and the control group were compared for the age, gestational age at delivery, and birth weight of the fetus (Figure 9). The birth weight of the fetus in the restricted group was significantly lower than that of the control group ($P < 0.05$). There was no statistical difference in gestational weeks ($P < 0.05$).

3.5. Analysis of Abnormal Results of Fetal Heart Rate Detection in the Two Groups. Figure 10 shows the abnormal fetal heart rate detection in the restricted group and the control group. There were 30 cases of the abnormal fetal heart rate in the restricted group, accounting for 73.17%; there were 17 cases of abnormal fetal heart rate in the control group, accounting for 41.46%. The proportion of fetal heart rate abnormalities in the restricted group was significantly higher than that in the control group and there was a statistical difference between the two ($P < 0.05$).

3.6. Comparison of Perinatal Outcomes between the Two Groups of Patients. Figure 11 shows the perinatal outcomes of the restricted group and the control group. There were 22

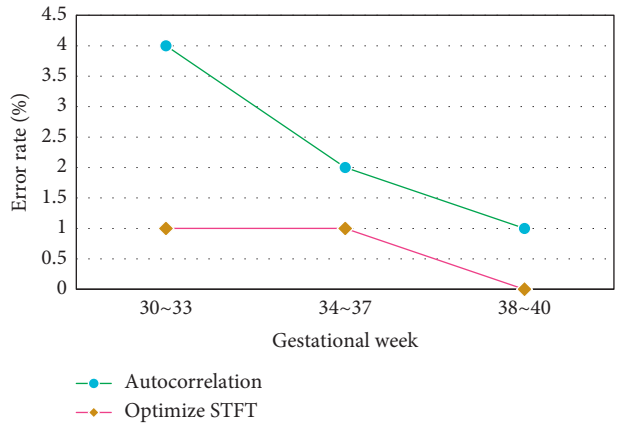

Figure 8: The fetal heart sound detection results by the optimized STFT algorithm.

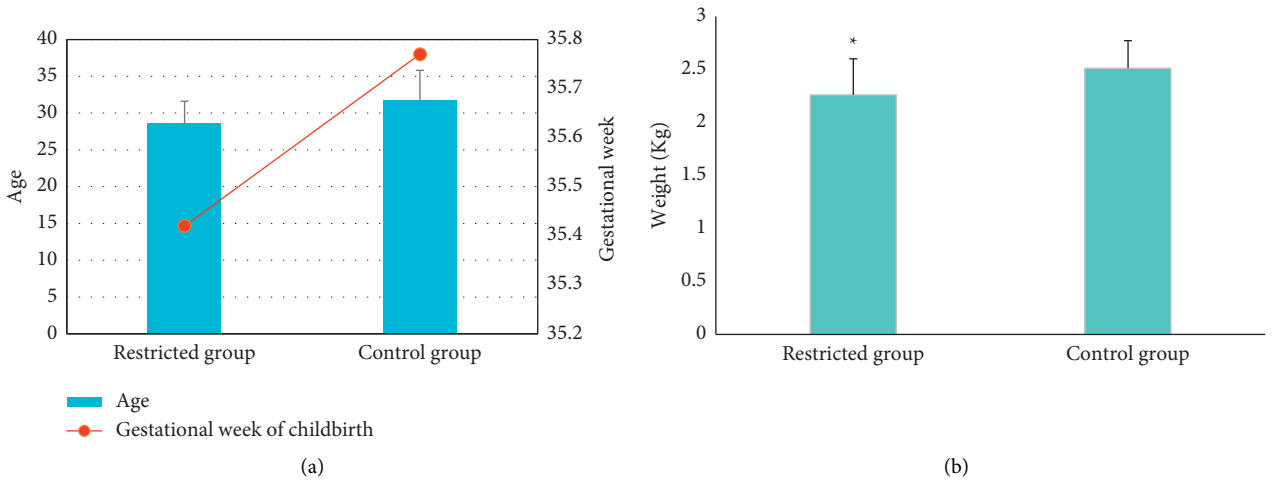

Figure 9: Comparison of basic data of pregnant women and fetuses between the two groups. (a) Comparison of age and gestational age between the two groups; (b) comparison of fetal weight at birth between the two groups (* represents a statistical difference compared with the control group, $P < 0.05$).

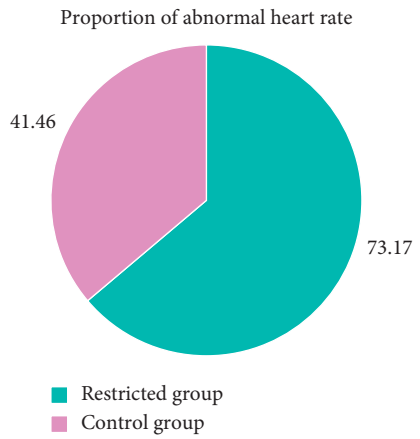

Figure 10: The proportion of patients with abnormal fetal heart rate in the two groups.

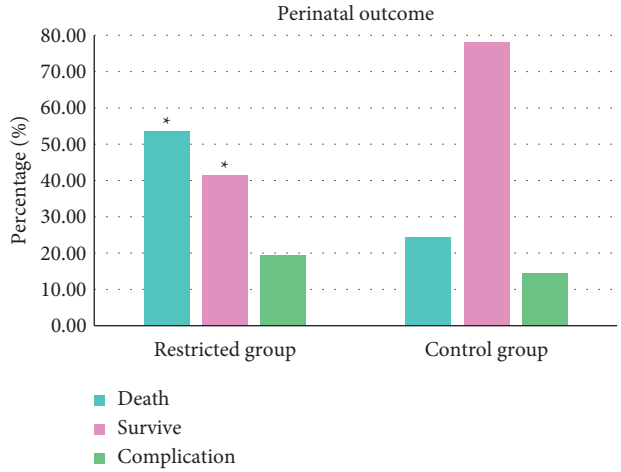

Figure 11: Comparison of perinatal outcomes between the two groups of patients (* indicates a significant difference compared with the control group, $P < 0.05$).

deaths and 17 survivors in the restricted group, accounting for 53.66% and 41.46%, respectively. There were 10 deaths and 32 survivors in the control group, accounting for 24.39% and 78.09%, respectively. The survival rate and mortality of the two groups were significantly different ($P < 0.05$). There was no statistical difference in the incidence of complications between the two groups ($P > 0.05$).

3.7. Analysis of sFas/sFasL Expression Levels in Cord Blood of the Two Groups. Figure 12 shows the sFas and sFasL expression levels. The sFas content of the restricted group was (3326.54 ± 317.42) pg/mL and the sFas content of the control group was (2003.29 ± 196.45) pg/mL. The sFas content of the restricted group was significantly higher than that of the control group ($P < 0.01$). The sFasL content of the restricted group was (382.52 ± 36.17) pg/mL and the sFasL content of the control group was (150.84 ± 16.20) pg/mL. The sFasL content of the restricted group was significantly higher than that of the control group ($P < 0.001$).

4. Discussion

In this study, the normalized image processing method was introduced into the STFT algorithm to optimize it to detect the fetal instantaneous heart rate. It was found that the cross-correlation coefficients were all above 0.86. The normalized cross-correlation algorithm is to calculate the correlation between vectors according to the row/column. A higher correlation coefficient indicates the correlation between the two images is better [17]. In the study, the correlation coefficients were all above 0.86, indicating that the normalized image processing method had a significant advantage in instantaneous heart rate extraction. The normal heart mainly includes four heart sounds S1~S4. In most cases, only two heart sounds S1 and S2 can be monitored by Doppler ultrasound [18]. In a cardiac cycle, the time characteristics of heart sounds can be fully expressed by the two heart sounds in systole S1 and diastolic S2 [19]. For normal fetuses, the normal heart rate is 120 to 160 beats/min [20]. The optimized STFT algorithm in this study can accurately segment the S1 and S2 fetal heart sounds. The detection error rates of the traditional autocorrelation algorithm at 32 weeks and 38 weeks were 4% and 2%, respectively. The detection error rates of the optimized STFT algorithm were 1% and 0, respectively, and the total detection error rate was reduced by 5%. These results showed that the optimized STFT algorithm had a significant advantage in instantaneous heart rate detection. It may be because the introduction of the normalized cross-correlation algorithm strengthens the accurate positioning performance of the fetal heart sound signal with a smaller amplitude and ultimately improves the calculation accuracy of fetal heart rates.

Fetal growth restriction is one of the important complications in the perinatal period. sIUGR can occur at any period of pregnancy and is one of the common complications in twin-to-twin pregnancy, mostly caused by congenital abnormalities. The results of this study found that the birth weight of the fetus in the restricted group was significantly lower than that in the control group ($P < 0.05$), indicating that the weight of the fetus in the restricted group was reduced. It may be related to the expected nutritional abundance, congenital abnormal diseases, and poor fetal development [21]. At the same time, the proportion of abnormal fetal heart rate in the restricted group was 73.17%, the proportion of abnormal fetal heart rate in the control group was 41.46%, and the proportion of abnormal fetal heart rate in the restricted group was significantly higher than that in the control group ($P < 0.05$), indicating that abnormal fetal heart rate can provide a reference for the diagnosis of twin-to-twin sIUGR. The abnormal fetal heart rate in the control group may be caused by the abnormal fetal blood supply and oxygen supply [22]. In the restricted group, there were 22 deaths and 17 survivors, accounting for 53.66% and 41.46%, respectively. In the control group, there were 10 deaths and 32 survivors, accounting for 24.39% and 78.09%, respectively. The survival rate and mortality of the two groups were significantly different ($P < 0.05$). There was no statistical difference in the incidence of complications between the two groups ($P > 0.05$). It showed that selective

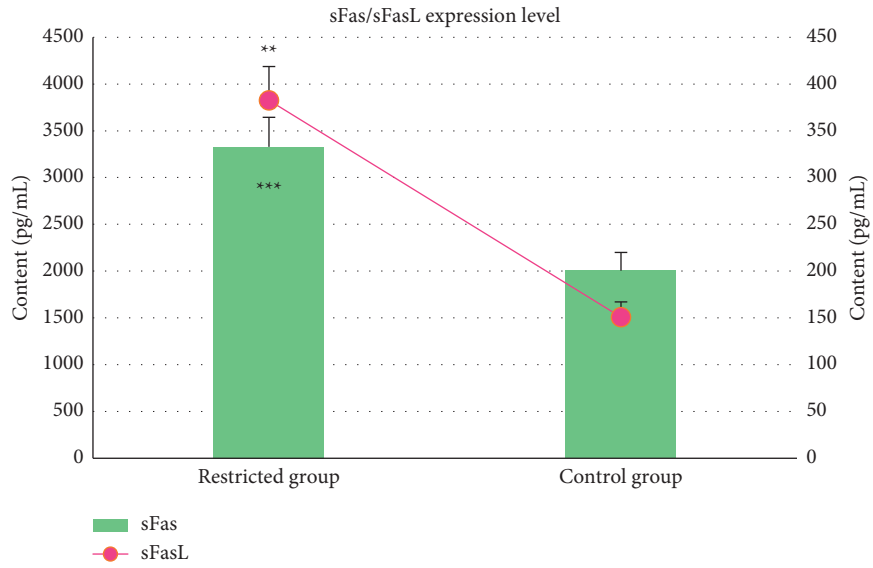

FIGURE 12: The expression levels of sFas/sFasL in cord blood of the two groups (** indicates a significant difference compared with the control group, $P < 0.01$; *** indicates a very significant difference compared with the control group, $P < 0.001$).

fetal restriction increased the mortality and survival rate of the fetus, so early ultrasound Doppler monitoring of the fetal heart rate is of great significance. The results in the study found that the sFas content of the restricted group was (3326.54 ± 317.42) pg/mL and the sFas content of the control group was (2003.29 ± 196.45) pg/mL. The sFas content of the restricted group was significantly higher than that of the control group ($P < 0.01$). The sFasL content of the restricted group was (382.52 ± 36.17) pg/mL and the sFasL content of the control group was (180.84 ± 16.20) pg/mL. The sFasL content of the restricted group was significantly higher than that of the control group ($P < 0.001$). sFas is a transmembrane glycoprotein, widely distributed in various tissues and organs of the human body, and plays an important role in cell apoptosis [23]. sFasL is the ligand of sFas, a member of the tumor necrosis factor superfamily, and is mainly expressed in activated lymphocytes [24]. The sFas/sFasL system can play a role in immune tolerance by mediating cell apoptosis, which is related to placental apoptosis [25]. The research of Karowicz et al. [26] pointed out that the expression of Fas in maternal blood of pregnant women with pregnancy-induced hypertension combined with sIUGR was significantly increased, the level of Fas of the fetus at birth was also significantly increased, and the expression of Fas in maternal blood was higher than that in cord blood ($P < 0.01$), consistent with the results of this study. Above, the changes in sFas/sFasL levels are correlated with the occurrence of sIUGR.

5. Conclusion

In the study, the normalized method was introduced into the STFT algorithm to optimize it to detect the fetal instantaneous heart rate and analyze the differences in the fetal mortality, complication rate, and cord blood sFas/sFasL expression levels between the restricted group and the control group. It was found that the optimized STFT in this study elevated the accuracy of fetal heart rate detection. The levels of sFas and sFasL had a certain correlation with twin-to-twin sIUGR. However, some limitations in the study should be noted. The sample size is small, the research subjects of this study have geographical limitations, which will reduce the power of the study. In the follow-up, an expanded sample size is necessary to strengthen the findings of the study. In conclusion, prenatal STFT-based ultrasound Doppler monitoring of fetal heart rate is conducive to early diagnosis and timely intervention in twin-to-twin sIUGR. The results that cell apoptosis increases in twin-to-twin sIUGR fetuses provide a reference for the diagnosis and treatment of twin-to-twin sIUGR.

Data Availability

The data used to support the findings of this study are available from the corresponding author upon request.

Conflicts of Interest

The authors declare no conflicts of interest.

References

[1] X. Huang, S. H. Saravelos, T. C. Li et al., "Cervical cerclage in twin pregnancy," *Best Practice & Research Clinical Obstetrics & Gynaecology*, vol. 59, pp. 89–97, 2019.

[2] B. Feng, J. Zhai, and Y. Cai, "Effect of twin pregnancy chorionic properties on maternal and fetal outcomes," *Taiwanese Journal of Obstetrics & Gynecology*, vol. 57, no. 3, pp. 351–354, 2018.

[3] L. M. M. Nardozza, A. C. R. Caetano, A. C. P. Zamarian et al., "Fetal growth restriction: current knowledge," *Archives of Gynecology and Obstetrics*, vol. 295, no. 5, pp. 1061–1077, 2017.

[4] M. C. Audette and J. C. Kingdom, "Screening for fetal growth restriction and placental insufficiency," *Seminars in Fetal and Neonatal Medicine*, vol. 23, no. 2, pp. 119–125, 2018.

[5] F. Gaccioli, I. L. M. H. Aye, U. Sovio, D. S. J. Charnock, and G. C. S. Smith, "Screening for fetal growth restriction using fetal biometry combined with maternal biomarkers," *American Journal of Obstetrics and Gynecology*, vol. 218, no. 2, pp. 725–737, 2018.

[6] P. Hamelmann, R. Vullings, A. F. Kolen et al., "Doppler ultrasound technology for fetal heart rate monitoring: a review," *IEEE Transactions on Ultrasonics, Ferroelectrics, and Frequency Control*, vol. 67, no. 2, pp. 226–238, 2020.

[7] X. Wang and K. Cai, "[Detection of heart rate of fetal ECG based on STFT and BSS]," *Zhongguo Yi Liao Qi Xie Za Zhi*, vol. 40, no. 1, pp. 22–26, 2016.

[8] C. Guo, J. Lu, Z. Tian, W. Guo, and A. Darvishan, "Optimization of critical parameters of PEM fuel cell using TLBO-DE based on Elman neural network," *Energy Conversion and Management*, vol. 183, pp. 49–158, 2019.

[9] K. Hirakawa, K. Koike, Y. Kanawaku et al., "Short-time fourier transform of free induction decays for the analysis of serum using proton nuclear magnetic resonance," *Journal of Oleo Science*, vol. 68, no. 4, pp. 369–378, 2019.

[10] Z. Lv and W. Xiu, "Interaction of edge-cloud computing based on SDN and NFV for next generation IoT," *IEEE Internet of Things Journal*, vol. 7, no. 7, pp. 5706–5712, 2020.

[11] D. T. Geddes and V. S. Sakalidis, "Ultrasound imaging of breastfeeding-A window to the inside," *Journal of Human Lactation*, vol. 32, no. 2, pp. 340–349, 2016.

[12] Y. Chen, S. Hu, H. Mao, W. Deng, and X. Gao, "Application of the best evacuation model of deep learning in the design of public structures," *Image and Vision Computing*, vol. 102, Article ID 103975, 2020.

[13] S. J. Cotton and W. H. Miller, "A symmetrical quasi-classical windowing model for the molecular dynamics treatment of non-adiabatic processes involving many electronic states," *The Journal of Chemical Physics*, vol. 150, no. 10, Article ID 104101, 2019.

[14] A. Kaso, "Computation of the normalized cross-correlation by fast Fourier transform," *PLoS One*, vol. 13, no. 9, Article ID e0203434, 2018.

[15] M. Bennasar, E. Eixarch, J. M. Martinez, and E. Gratacós, "Selective intrauterine growth restriction in monochorionic diamniotic twin pregnancies," *Seminars in Fetal and Neonatal Medicine*, vol. 22, no. 6, pp. 376–382, 2017.

[16] R. L. T. Bevan, J. Zhang, N. Budyn, A. J. Croxford, and P. D. Wilcox, "Experimental quantification of noise in linear ultrasonic imaging," *IEEE Transactions on Ultrasonics, Ferroelectrics, and Frequency Control*, vol. 66, no. 1, pp. 79–90, 2019.

[17] R. H. Chmait, A. H. Chon, L. M. Korst, Y. Stephen, A. Llanes, and J. G. Ouzounian, "Selective intrauterine growth restriction (SIUGR) type II: proposed subclassification to guide surgical management," *Journal of Maternal-Fetal and Neonatal Medicine*, vol. 31, pp. 1–8, 2020.

[18] C. Xiefeng, Y. Wang, S. Dai, P. Zhao, and Q. Liu, "Heart sound signals can be used for emotion recognition," *Scientific Reports*, vol. 9, no. 1, 2019.

[19] C. Will, K. Shi, S. Schellenberger et al., "Radar-based heart sound detection," *Scientific Reports*, vol. 8, no. 1, Article ID 11551, 2018.

[20] J. Wei, Z. Wang, and X. Xing, "A wireless high-sensitivity fetal heart sound monitoring system," *Sensors*, vol. 21, no. 1, 2020.

[21] M. Colella, A. Frérot, A. R. B. Novais, and O. Baud, "Neonatal and long-term consequences of fetal growth restriction," *Current Pediatric Reviews*, vol. 14, no. 4, pp. 212–218, 2018.

[22] M. A. Pedroso, K. R. Palmer, R. J. Hodges, F. D. S. Costa, and D. L. Rolnik, "Uterine artery Doppler in screening for pre-eclampsia and fetal growth restriction," *Revista Brasileira de Ginecologia e Obstetrícia: revista da Federacao Brasileira das Sociedades de Ginecologia e Obstetricia*, vol. 40, no. 5, pp. 287–293, 2018.

[23] A. Y. Su, X. Z. Yang, M. H. Zhang, Z. X. Di, and Q. Li, "[Analysis of correlation of immune T cell subsets, TNF-α, IFN-γ and sFas levels with severity and prognosis in aplastic anemia patients]," *Zhongguo Shi Yan Xue Ye Xue Za Zhi*, vol. 26, no. 5, pp. 1459–1464, 2018.

[24] M. Wang and P. Su, "The role of the Fas/FasL signaling pathway in environmental toxicant-induced testicular cell apoptosis: an update," *Systems Biology in Reproductive Medicine*, vol. 64, no. 2, pp. 93–102, 2018.

[25] B. L. Liphaus, M. H. B. Kiss, S. Carrasco, P. Palmeira, C. S. Goldenstein, and M. S. Carneiro, "Increased serum sFas, sTRAIL, and reduced sFasL in juvenile-onset systemic lupus erythematosus," *Clinical Rheumatology*, vol. 36, no. 12, pp. 2847–2852, 2017.

[26] A. B. Karowicz, U. K. Kowalska, D. Estemberg, and A. S. Sikora, "Evaluation of soluble concentration Fas and Fas ligand in maternal and cord blood 3rd trimester of pregnancy," *Ginekologia Polska*, vol. 89, no. 3, pp. 142–146, 2018.